Published in final edited form as:

Biomacromolecules. 2017 December 11; 18(12): 4075–4083. doi:10.1021/acs.biomac.7b01155.

Porous PCL-PLLA semi-IPNs as superior, defect-specific scaffolds with potential for cranial bone defect repair

Lindsay N. Woodard[1], **Kevin T. Kmetz**[1], **Abigail A. Roth**[1], **Vanessa M. Page**[1], and **Melissa A. Grunlan**[1,2,*]

[1]Department of Biomedical Engineering, Texas A&M University, College Station, Texas 77843, USA.

[2]Department of Material Science and Engineering, Texas A&M University, College Station, Texas 77843, USA.

Abstract

The treatment of irregular cranial bone defects is currently limited due to the graft resorption that can occur when an ill-fitting interface exists between an autograft and the surrounding tissue. A tissue engineering scaffold able to achieve defect-specific geometries could improve healing. This work reports a macroporous, shape memory polymer (SMP) scaffold composed of a semi-interpenetrating network (semi-IPN) of thermoplastic poly(L-lactic acid) (PLLA) within cross-linked poly(ε-caprolactone) diacrylate (PCL-DA) that is capable of conformal fit within a defect. The macroporous scaffolds were fabricated using a fused salt template and were also found to have superior, highly-controlled properties needed for regeneration. Specifically, the scaffolds displayed interconnected pores, improved rigidity and controlled, accelerated degradation. While slow degradation rates of scaffolds can limit healing, the unique degradation behavior observed could prove promising. Thus, the described SMP semi-IPN scaffolds overcome two of the largest limitations in bone tissue engineering – defect "fit" and tailored degradation.

Keywords

Bone tissue engineering; shape memory polymers; semi-interpenetrating networks; poly(ε-caprolactone); poly(L-lactic acid); degradation

INTRODUCTION

The treatment of confined cranial bone defects remains limited in part due to the challenge of shaping and fitting autologous tissue tightly within an irregular defect.[1] An insufficient

*Corresponding Author mgrunlan@tamu.edu.

Author Contributions

The manuscript was written through contributions of all authors. All authors have given approval to the final version of the manuscript.

ASSOCIATED CONTENT

Supporting Information

TGA confirming PCL-PLLA semi-IPN composition; effect of annealing temperature on PCL-DA (n = 45) scaffolds (2); validation of response-to-annealing hypothesis via PCL-PDLLA scaffold porosity; scaffold compressive strength with annealing temperature; table containing key PCL-PLLA semi-IPN scaffold properties; scaffold morphology via SEM; scaffold shape-fitting demonstration (PDF).

interface between the graft and the contours of the defect contributes to poor healing outcomes due to graft resorption.[2] Current alternatives to autologous tissue include materials with poor handing and high exothermic temperatures during curing, with a majority of the interventions involving permanent, non-degradable tissue replacements.[3]

Regenerative engineering aims to restore native tissue and function via a scaffold to guide and support repair.[3c, 4] Such a scaffold must (1) have interconnected macropores to facilitate osteoconduction, (2) be mechanically robust as to prevent collapse or brittle fracture, (3) biodegrade with neotissue formation and (4) conform to the adjacent bone tissue, permitting osseointegration. Many scaffold approaches, however, do not prioritize obtaining high contact with the defect boundaries. The development of scaffolds that are able to achieve defect geometries remains hindered by complex in situ cure, a lack of containment and control upon implantation, as well as cost and time restrictions.[5] Thus, a scaffold that is able to effectively support tissue repair via conformal fit within a cranial defect could greatly improve treatment outcomes.

Thermoresponsive shape memory polymers (SMPs) are capable of shape change in response to thermal stimuli due to the accompanied changes of “switching segments” (e.g. amorphous or crystalline polymer domains). “Netpoints” (e.g. chemical or physical cross-links), then, define the permanent shape.[6] SMPs have been explored for a variety of biomedical applications.[6–7] While some applications include porous scaffolds for tissue engineering,[8] SMP behavior was not utilized to achieve conformal defect fitting. Recently, we have reported an SMP scaffold able to be molded and shaped to the contours of a model defect.[9] When heated ($T > T_{trans}$), the scaffold becomes deformable and is able to be easily press-fitted tightly within a defect. Then, upon cooling ($T < T_{trans}$), the scaffold returns to its original, rigid state, in its new shape, fixed within the defect. This “self-fitting” scaffold approach is the only ex vivo-fabricated approach, other than via solid freeform (SFF) fabrication,[4] able to achieve patient-specific geometries. Notably, scaffold properties (e.g. open pore morphology) are maintained during the shaping and fitting process.[9a]

Our previously-reported scaffolds were based on networks formed via the cross-linking of poly(ε-caprolactone) diacrylate (PCL-DA). In addition to the, albeit slow, biodegradability of PCL, by utilizing the melting temperature (T_m) of PCL as T_{trans}, scaffold malleability can be achieved ~55 °C – a mild temperature relative to other thermoplastic SMPs.[10] Herein, we sought to expand the mechanical properties and degradation rates of the PCL-DA scaffolds by incorporating a second polymer component. Due to the relatively low stiffness of PCL,[10b] combinations of PCL with mechanically rigid polymers have attracted general attention for obtaining improved, synergistic mechanical properties.[11] Poly(L-lactic acid) (PLLA) has been a popular choice given its high modulus of ~2.7 GPa due to semi-crystallinity and a high glass transition temperature (T_g) of ~60 °C.[10b, 12] Furthermore, PLLA is also known to degrade within 1–2 years compared to PCL’s reported 2+ years.[13]

Scaffold approaches based on a combination of PCL and PLLA have been limited largely to blending and copolymerization.[13–14] In addition to lacking shape memory behavior, these approaches have had underwhelming success *in vivo* due to limited, slow rates of degradation.[15] In this work, semi-interpenetrating polymer networks (semi-IPNs) were

prepared comprised of cross-linked PCL-DA and thermoplastic PLLA. Numerous biomaterial semi-IPNs have been investigated in recent years,[16] and some exhibited improved properties over analogous polymer blends.[17] Yet, there are only sparse reports of bulk (i.e. non-porous) PCL-PLLA semi-IPNs,[18] and the molecular structure has not been explored as an SMP or as a porous SMP scaffold.

In a recent study, we prepared bulk SMP semi-IPNs based on PCL-DA and PLLA at varying weight % ratios of the two components.[19] These semi-IPNs maintained shape memory behavior and displayed tunable, accelerated rates of degradation as well as, for some compositions, increased stiffness and strength. In the current study, porous PCL-PLLA semi-IPN scaffolds were investigated. A solvent-casting particulate-leaching (SCPL) fabrication technique, previously shown to produce interconnected macropores, was utilized.[9a, 20] Based on the molecular design and macroporosity, it was expected that the scaffolds would possess the requisite properties for tissue regeneration while also being capable of achieving a defect-specific “fit” during implantation (Figure 1). Semi-IPN PCL:PLLA weight % ratios (100:0 [PCL-DA control], 90:10, 75:25, 60:40) and PCL-DA average degree of polymerization (n) were varied (n = 25, 45). The PLLA average degree of polymerization (m) was maintained at m = 90. Scaffold thermal properties (crystallinity and T_m), shape memory behavior, degradation rates and mechanical properties (stiffness and strength) were assessed along with analysis of the effect of annealing temperature on scaffold morphology.

EXPERIMENTAL SECTION

Materials

Polycaprolactone diol (PCL_{90}-diol; M_n ~10,000 g mol^{-1}), ε-caprolactone, L-lactide, D,L-lactide, stannous 2-ethylhexanoate, triethylamine (Et_3N), acryloyl chloride, 4-dimethylaminopyridine (DMAP), 2,2-dimethoxy-2-phenylacetophenone (DMP), 1-vinyl-2-pyrrolidinone (NVP), potassium carbonate (K_2CO_3), sodium hydroxide (NaOH), sodium chloride (NaCl), ethylene glycol and solvents were obtained from Sigma-Aldrich. Anhydrous magnesium sulfate ($MgSO_4$) was obtained from Fisher. Reagent-grade CH_2Cl_2 and NMR-grade $CDCl_3$ were dried over 4 Å molecular sieves prior to use.

Material Synthesis

PCL_{2n}-diol (n = 25) and $PLLA_{2m}$-diol (m = 90) were synthesized as previously reported.[19] Briefly, PCL_{2n}-diol and $PLLA_{2m}$-diol were prepared by the ring-opening polymerization of ε-caprolactone or L-lactide, respectively, with ethylene glycol as the initiator and stannous 2-ethylhexanoate catalyst. $PDLLA_{2m}$-diol from D,L-lactide was similarly prepared. The terminal hydroxyl groups of PCL_{2n}-diol (n = 25, 45) were then reacted with acryloyl chloride, resulting in photosensitive acrylate (OAc) groups. The number average molecular weights (M_n) and degrees of acrylation were determined by ^1H NMR and were in agreement with those previously reported.[19]

Fabrication

Porous scaffolds were prepared via a previously-described SCPL method.[9a, 20]—To prepare a fused salt template, NaCl particles were first collected from a sieve

with 425 μm openings, resulting in 527 ± 92 μm particles, as determined with ImageJ software from scanning electron microscopy (SEM) images. For each scaffold, 1.8 g NaCl was placed within a 3 mL glass vial and fused via treatment with 7.5 wt% of DI water. The water was gradually added to the NaCl particles and mechanically stirred prior to centrifugation (3,220 G, 15 min). After air-drying (RT, 1 h), the NaCl templates were dried *in vacuo* (RT, 12 h).

Solutions (0.15 g mL^{-1} CH_2Cl_2) of PCL:PLLA (100:0 [PCL-DA control], 90:10, 75:25, 60:40 wt% ratio) were prepared with 15 vol% of a photoinitator solution (10 wt% DMP in NVP). PCL:PDLLA (75:25 wt% ratio) solutions were also prepared to serve as a control. The precursor solutions were added to the fused NaCl template, to cover (~0.6 mL). The vial was then centrifuged (1,260 G, 10 min) and exposed to UV light (UV-Transilluminator, 6 mW cm^{-2}, 365 nm) for 3 min. After air-drying (RT, 12 h), the SMP scaffold was removed from the vial, and the NaCl was leached by soaking in a water/ethanol mixture (1:1 vol:vol) for 4 days with daily solution changes. Upon removal and air-drying (RT, 12 h), the resulting scaffold was annealed at either 85 °C for 1 h (*in vacuo*) or 160 °C for 10 min (*in vacuo*) and allowed to set at RT for 48 h prior to testing.

SMP Characterization

Semi-IPN Composition—Thermogravimetric analysis (TGA, TA Instruments Q50) of specimens (~10 mg, $N = 1$) in platinum pans was run under N_2 from RT to 500 °C at a heating rate of 10 °C min^{-1}. The mass of the samples throughout heating was measured to quantify percent mass remaining.

Porosity—The % porosity of the SMP scaffolds ($N = 4$) was determined by:

$$P(\%) = \frac{\rho_{solid\ SMP} - \rho_{porous\ SMP}}{\rho_{solid\ SMP}} \times 100$$

For each scaffold composition, the density (ρ) of the corresponding bulk (i.e. non-porous) film was gravimetrically determined to be, for PCL-DA (n = 25), 1.158, 1.158, 1.182, 1.134 g cm^{-3} and, for PCL-DA (n = 45), 1.175, 1.164, 1.220, 1.163 g cm^{-3}, respectively.

Pore Size and Morphology—Scaffold pore size and pore interconnectivity were evaluated via SEM. Scaffolds cross sections were subjected to Au-Pt coating (~4 nm). Images were obtained using a JEOL 6400 SEM with an accelerating voltage of 10 kV. From the SEM images ($N = 4$), the average pore size was determined from pores measured along each image midline with ImageJ software.

Thermal Properties—The T_m and % crystallinity of each semi-IPN component was determined by differential scanning calorimetry (DSC, TA Instruments Q100). Scaffold specimens (~10 mg; $N = 3$) sealed in hermetic pans were heated from RT to 200 °C at a heating rate of 5 °C min^{-1}. From the endothermic PCL and PLLA melting peaks, T_m and enthalpy change (ΔH_m) were measured. Percent crystallinity (% χ_c) was calculated via:

$$\% \ \chi_c = \frac{\Delta H_m}{\Delta H_m^o} \times 100$$

where ΔH_m was calculated by the area of the melting peak, and $\Delta H°_m$ is the enthalpy of fusion of 100% crystalline PCL (139.5 J g^{-1})[21] or PLLA (93.0 J g^{-1}).[22]

Shape Memory Behavior—Shape memory behavior was quantified via a strain-controlled cyclic-thermal mechanical test in compression over two cycles (N) (dynamic mechanical analysis [DMA], TA Instruments Q800). The scaffold cylinders ($N = 4$) were subjected to the following program: (1) After equilibrating to 60 °C (T_{high}) for 5 min, compress to a maximum strain (ε_m = 50%) at a rate of 50% min^{-1}, (2) hold at ε_m for 5 min, then cool to 25 °C (T_{low}) to fix the temporary shape, (3) remove the load and immediately measure ε_u and (4) reheat to 60 °C (T_{high}) to recover the permanent shape, measure the recovered strain (ε_p). The shape fixity (R_f) and shape recovery (R_r) for the first (N = 1) and second (N = 2) cycles were calculated, respectively, via:

$$R_f(N) = \frac{\varepsilon_u(N)}{\varepsilon_m}$$

$$R_r(N) = \frac{\varepsilon_m - \varepsilon_p(N)}{\varepsilon_m - \varepsilon_p(N-1)}$$

where $\varepsilon_u(N)$ is the strain in the stress-free state of the fixing process, ε_m is the maximum compressive strain (50%) and $\varepsilon_p(N-1)$ and $\varepsilon_p(N)$ are the final recovered strains of the scaffolds in the two sequential cycles. For N = 1, $\varepsilon_p(0)$ equaled "zero."

Accelerated Degradation—Scaffolds ($N = 4$, per time point) were each immersed in 20 mL of 1 M NaOH in a sealed centrifuge tube maintained at 37 °C. At 8, 24, 72 and 168 h, the corresponding samples were taken from solution, thoroughly rinsed with DI water, blotted and dried *in vacuo* (RT, 12 h). The mass of the dried scaffolds was then gravimetrically determined.

Mechanical Properties—Compressive properties were evaluated at RT with an Instron 3345. Scaffold cylinders ($N = 5$) were subjected to a constant strain rate (1.5 mm min^{-1}) up to 85% strain (ε). From the resulting stress-strain curves, modulus (E) was determined as the slope in the initial linear region (< ~10% ε). Compressive strength at 85% ε was also determined.

Statistical Analysis—Data was reported as the mean ± standard deviation. Values were compared using ANOVA with Dunnett post-hoc to determine *p*-values.

RESULTS AND DISCUSSION

Porous scaffolds were fabricated of semi-IPNs containing PCL-DA and PLLA in varying PCL:PLLA wt% ratios via SCPL in which precursor solutions were photocured around a fused NaCl template (Figure 1). Previous work investigating bulk PCL-PLLA semi-IPNs confirmed that the presence of PLLA did not diminish the cross-linking of PCL-DA.[19] As for bulk semi-IPNs,[19] TGA was used to verify the scaffold semi-IPN PCL:PLLA wt% ratio. Despite the leaching of the NaCl template, TGA confirmed that the composition of precursor solutions was maintained in the scaffolds (Figure S1).

Effect of Annealing Temperature

In previous work,[9a] it was found that annealing porous PCL-DA scaffolds at 85 °C ($T > T_{m,PCL}$) caused concomitant densification (i.e. shrinkage) and was required for shape memory behavior. The annealing was speculated to provide the necessary increased proximity of PCL crystalline domains (i.e. “switching segments”). In this work, with the addition of semi-crystalline PLLA ($T_{m,PLLA}$ ~155 °C) to form the PCL-PLLA semi-IPNs, analysis of annealing temperature on scaffold densification was warranted. Thus, an additional annealing temperature of 160 °C ($T > T_{m,PCL}$ & $T > T_{m,PLLA}$) was investigated. In addition to noting the scaffold dimensions before and after annealing (at 85 °C or 160 °C), average pore size, scaffold porosity (%) and the resulting mechanical properties were also quantified.

First, scaffold diameter was observed following annealing at 85 °C and 160 °C. Prior to annealing, all scaffold compositions exhibited the same diameter due to their fabrication in molds of the same diameter (Figure 2a). For semi-IPNs scaffolds prepared with PCL-DA (n = 25), when annealed at 85 °C, the extent of shrinkage decreased with PLLA content. In this way, the 60:40 (PCL:PLLA wt%) semi-IPN scaffold underwent the least amount of densification upon annealing. However, when annealed at 160 °C, scaffolds of all semi-IPN compositions shrunk to a diameter similar to that of the PCL-DA control. As expected, the extent of densification affected pore size, as revealed by SEM (Figure 2b). Prior to annealing, all scaffold compositions exhibited large pores of similar size (~349 μm) (Figure 2c). Upon annealing at 85 °C, pore size decreased, and the resulting average pore size varied with PCL:PLLA wt% ratio. When compared to the average pore size of the PCL-DA control (~231 μm), the corresponding semi-IPN scaffolds contained significantly larger average pore sizes (247–338 μm) that increased with PLLA content. In contrast, scaffolds annealed at 160 °C exhibited similar average pore sizes of ~214 μm for all compositions. Similar observations were made for PCL-DA control and semi-IPN scaffolds prepared with PCL-DA (n = 45) (Figure S2).

We attribute the above findings to differences in crystalline domain melting, and subsequent chain mobility, when annealed at 85 °C versus 160 °C (Figure 2d). We hypothesize that a temporary loss in crystallinity upon melting allows for chain reorganization and general movement into the pore spaces. Thus, when annealed at 160 °C ($T > T_{m,PCL}$ & $T > T_{m,PLLA}$), chain reorganization is enhanced for both PCL and PLLA, resulting in similarly sized, smaller pores independent of PLLA content. In contrast, upon annealing at 85 °C ($T > T_{m,PCL}$), PLLA crystalline regions do not melt. Reorganization occurs, yet is restricted by

the PLLA crystallinity, resulting in composition-dependent pore size and accompanying densification. In support of this hypothesized mechanism, scaffolds prepared with amorphous poly(D,L-lactic acid) (PDLLA) (75:25 [PCL:PDLLA wt%]), and likewise annealed at 85 °C, exhibited scaffold porosity similar to that of a PCL-DA control (Figure S3).

In addition to evaluating scaffold densification and pore size, scaffold % porosity was also quantified (Figure 3a). Prior to annealing, the % porosities of PCL-DA control and PCL-PLLA semi-IPN scaffolds (PCL-DA; n = 25) were similar (~89%). Overall, % porosity decreased upon annealing due to the reduction in pore size, the extent of which depended on annealing temperature, as noted above. For scaffolds annealed at 85 °C, porosity remained greatest with increased levels of PLLA. Specifically, semi-IPN scaffold % porosities ranged from ~76 to 86% versus ~71% for the PCL-DA control. However, when annealed at 160 °C, the porosities of all scaffolds decreased to ~66% independent of PCL:PLLA wt% ratio.

As porosity is often regarded as the greatest contributor to cellular solid mechanical properties,[23] scaffold % porosity was considered when initially evaluating compressive modulus (E) and compressive strength (CS). Prior to annealing, the PCL-DA control and PCL-PLLA semi-IPN (PCL-DA; n = 25) scaffolds exhibited similar E values of ~0.5 MPa (Figure 3b). Upon annealing, all scaffold moduli were substantially increased due to the described densification. For 85 °C-annealed semi-IPN scaffolds, modulus values were less than the PCL-DA control (E = 13.9 MPa) and decreased with PLLA content (E = ~9.2–1.8 MPa). We attribute this decline in E to the greater % porosities for PLLA-containing scaffolds. After annealing at 160 °C, scaffolds exhibit similar % porosities such that E values were coupled to only composition. For these scaffolds, E increased with PLLA content, reaching a maximum value of E = ~21 MPa for 75:25 and 60:40 (PCL:PLLA wt%) semi-IPN scaffolds. For scaffolds prepared with PCL-DA (n = 45), similar trends in % porosity and mechanical properties were seen (Figure S4, Figure S5).

To summarize, annealing temperature drastically influenced average pore size and % porosity. When annealed at 85 °C, scaffold pore size and % porosity increase with PLLA content. However, after annealing at 160 °C, all scaffolds conveniently exhibit similar pore size and % porosity, permitting scaffold properties to be evaluated exclusively in terms of composition. Thus, 160 °C was utilized for subsequent characterization of scaffolds.

Semi-IPN Scaffold Characterization

The macroporous morphology of the scaffolds can be attributed to the SCPL fabrication. Upon annealing at 160 °C, scaffolds consisted of 208 ± 9.6 μm pores and a porosity of ~67%, which was independent of PCL:PLLA wt% ratio and PCL-DA ‘n’ (Figure S6, Table S1). Because the NaCl particles used during scaffold fabrication were of controlled size (527 ± 92 μm), pore size deviation within a scaffold was minimal. Additionally, as the NaCl particles were fused into a continuous template during fabrication, scaffolds exhibited a high degree of pore interconnectivity.

Scaffold crystallinity is of great importance as it ultimately influences shape memory behavior, degradation and scaffold mechanical properties. Thus, % crystallinity and the

associated T_m of both semi-IPN components were determined for all scaffold compositions (Figure 4a, Table S1). The crystalline domains of PCL serve as "switching segments" and accordingly enable shape memory behavior. PCL semi-crystallinity was exhibited for all semi-IPN scaffolds despite the presence of thermoplastic PLLA and reported suppression of crystallinity when cross-linked.[24] Similar to bulk PCL-PLLA semi-IPNs,[19] a reduction in PCL crystallinity was seen with increased PLLA content in the scaffolds. PLLA semi-crystallinity was also observed for all semi-IPN scaffold compositions and increased with PLLA content. Differences in crystallinity values between scaffolds based on PCL-DA (n = 25) versus PCL-DA (n = 45) were minor. Notably, scaffolds exhibited a $T_{m,PCL}$ (i.e. T_{trans} for shape memory) of ~54 °C and ~56 °C for scaffolds of PCL-DA (n = 25) and PCL-DA (n = 45), respectively, independent of PLLA content.

SMP behavior via "switching segments" (i.e. PCL crystalline domains) and "netpoints" (i.e. PCL-DA network covalent cross-links) provides the ability of the scaffolds to be molded into a defect-specific shape upon implantation. A standard, strain-controlled cyclic-thermal mechanical test was utilized to quantify the shape memory properties of the scaffolds. Both shape fixity (R_f) (i.e. the ability of the scaffold to retain a temporary shape when $T < T_{trans}$) and shape recovery (R_r) (i.e. the ability of the scaffold to return to its original shape when $T > T_{trans}$) were quantified over two test cycles (Figure 4b). All scaffolds showed excellent R_f values of 100.6–101.9% for both cycles. R_f values slightly greater than 100% have been previously observed for porous PCL-based materials and can be attributed to the rapid crystallization of PCL upon cooling.[25] High R_f values indicate that the scaffolds should effectively retain a new, fixed shape within an irregular defect. R_r values were composition and cycle dependent. For scaffolds based on both PCL-DA (n = 25) and PCL-DA (n = 45), R_r was reduced for PLLA-containing semi-IPN scaffolds compared to PCL-DA controls and decreased with increased PLLA content. We hypothesize that during shape recovery at 60 °C, PLLA remained semi-crystalline (60 °C < $T_{m,PLLA}$), reducing the mobility of the PCL "switching segments." Particularly during the first cycle, scaffolds based on PCL-DA (n = 25) consistently exhibited greater R_r values compared to scaffolds based on PCL-DA (n = 45). It is hypothesized that the higher cross-link density and reduced chain length of PCL-DA (n = 25) promotes cooperative interaction within the switching domains. Importantly, as is commonly observed for porous SMP systems,[23a, 26] R_r values increased from the first to the second cycle. By the second cycle, all semi-IPN scaffolds recovered to at least ~90%. This indicates that scaffolds would undergo a high degree of expansion to fill irregular defects.

A simulation of scaffold implantation was performed with an irregular model cranial defect (Figure 4c). Scaffolds were initially prepared in a generic shape (cylinder, 12 × 5 mm). Upon exposure to ~60 °C saline, the scaffold became malleable and allowed for facile press-fitting within the model defect. Upon cooling, the defect-specific shape was fixed, even after removal from the mold. The ability of these scaffolds to "fix" other various shapes was also demonstrated (Figure S7).

Scaffold degradation was evaluated under accelerated conditions (1 M NaOH, 37 °C) via mass loss and visual observation (Figure 5). PCL-PLLA semi-IPN scaffolds lost mass much more quickly than the corresponding PCL-DA control scaffold, and the rate of mass loss

increased with PLLA content. For instance, at 24 h, the observed mass loss for semi-IPN scaffolds was ~16–100% (PCL-DA; n = 25) and ~23–79% (PCL-DA; n = 45) versus ~9% and ~3% for PCL-DA control scaffolds, respectively. Acceleration in degradation was likewise observed for bulk PCL-PLLA semi-IPNs,[19] as well as for blends and copolymers of PLLA and PCL.[27] We hypothesize that phase separation and a reduced PCL crystallinity further promote solution diffusion, and subsequent hydrolysis, for the PCL–PLLA semi-IPNs over PCL-DA controls. Additionally, scaffolds prepared with PCL-DA (n = 25) exhibited accelerated degradation versus scaffolds prepared with PCL-DA (n = 45). We attribute this to the greater number of hydrolytically-liable bonds within the acrylate cross-links in the high cross-link density network. In total, the series of semi-IPNs provide a wide range of degradation rates. Interestingly, mass loss resulted in a decrease of scaffold dimensions without breakage into smaller pieces (Figure 5c). This observation of surface erosion would be unexpected given that PCL and PLLA are each known to degrade via bulk erosion.[10b] The erosion behavior of the scaffolds may be attributed to the alkaline testing conditions,[28] although such testing conditions are often utilized to initially assess scaffold degradation properties.[25, 29]

The compressive modulus (E) and compressive strength (CS) of the scaffolds were determined from stress-strain curves obtained via typical compression testing (Figure 6, Table S1).[13, 25] For semi-IPN scaffolds based on PCL-DA (n = 25), E values were higher for PCL:PLLA wt% ratios of 75:25 (E = 20.7 MPa) and 60:40 (E = 21.4 MPa) versus the PCL-DA control (E = 13.0 MPa). When based on PCL-DA (n = 45), modulus also increased for a PCL:PLLA wt% ratio of 75:25 (E = 19.3 MPa) versus the PCL-DA control (E = 16.6 MPa). This increase in E with greater PLLA content is attributed to the rigidity of high-T_g, semi-crystalline PLLA. However, the semi-IPN scaffold based on PCL-DA (n = 45) with a PCL:PLLA wt% ratio of 60:40 (E = 15.8 MPa) was similar to that of the PCL-DA control (E = 16.6 MPa). Thus, a combination of cross-link density and % crystallinity influence modulus values. Scaffold CS at 85% ε was similar between PCL-DA controls and PCL-PLLA semi-IPN scaffolds. Versus the PCL-DA control (n = 25; CS = 20.5 MPa), only the semi-IPN scaffold with a PCL:PLLA wt% ratio of 75:25 (CS = 24.8 MPa) showed an increase in strength. For a given PCL:PLLA wt% ratio, CS values were typically higher for scaffolds prepared with PCL-DA (n = 45) versus PCL-DA (n = 25). This was also observed for bulk semi-IPN analogues and indicates that a reduced cross-link density may permit additional chain deformation and subsequent chain alignment to achieve higher stress values.[19]

CONCLUSIONS

Scaffolds capable of achieving a conformal fit in irregular cranial defects are expected to improve osteointegration and, thus, healing. In this work, porous scaffolds able to achieve defect-specific geometries via shape memory behavior were described. The scaffolds, comprised semi-IPNs of cross-linked PCL-DA and thermoplastic PLLA, were prepared and their key properties investigated. The annealing temperature used during scaffold fabrication was found to have a significant effect on scaffold properties. When annealed at 85 °C, the average pore size and % porosity were dependent on the PCL:PLLA wt% ratio. When

annealed at 160 °C, average pore size and % porosity were consistent between scaffolds, allowing for effective evaluation of scaffold properties based solely on composition.

Essential for tissue regeneration, all semi-IPN scaffolds exhibited both macroporosity and pore interconnectivity. Due to PCL semi-crystallinity (i.e. PCL “switching segments”; $T_{m,PCL} = T_{trans}$), shape memory behavior was realized for the scaffolds, particularly by the second cycle. Towards a mechanically robust scaffold, higher modulus values were achieved for some semi-IPN scaffolds versus PCL-DA controls. For instance, when prepared with PCL-DA (n = 25), a ~62% increase in modulus was observed for the semi-IPN scaffolds having PCL:PLLA wt% ratios of 75:25 and 60:40. Modest increased in strength was also observed for some semi-IPN scaffolds. Notably, scaffolds demonstrated controlled and substantially accelerated rates of degradation that corresponded with both PCL:PLLA wt% ratio and PCL ‘n.’ Thus, a comprehensive scaffold capable of excellent defect “fit” for improved cranial bone defect repair has been described.

Supplementary Material

Refer to Web version on PubMed Central for supplementary material.

ACKNOWLEDGMENT

Funding from NIH NIDCR 1R01DK095101–01A1 and the NSF Graduate Research Fellowship Program (NSF GRFP) (L.W.) is gratefully acknowledged.

Funding Sources

NIH NIDCR 1R01DK095101–01A1

NSF Graduate Research Fellowship Program (NSF GRFP) (L.W.)

REFERENCES

1. (a) Neovius E; Engstrand T, Craniofacial reconstruction with bone and biomaterials: review over the last 11 years. J. Plast. Reconstr. Aesthet. Surg. 2010, 63 (10), 1615–1623; [PubMed: 19577527] (b) Kellman RM, Safe and dependable harvesting of large outer-table calvarial bone grafts. Arch. Otolaryngol. Head Neck Surg. 1994, 120 (8), 856–860; [PubMed: 8049049] (c) Kinoshita Y; Maeda H, Recent developments of functional scaffolds for craniomaxillofacial bone tissue engineering applications. Scientific World J. 2013, 2013, 1–21.
2. (a) Alsberg E; Hill E; Mooney D, Craniofacial tissue engineering. Crit. Rev. Oral Biol. M. 2001, 12 (1), 64–75; [PubMed: 11349963] (b) Moreira-Gonzalez A; Jackson IT; Miyawaki T; Barakat K; DiNick V, Clinical outcome in cranioplasty: critical review in long-term follow-up. J. Craniofac. Surg. 2003, 14 (2), 144–153; [PubMed: 12621283] (c) Lee SH; Yoo CJ; Lee U; Park CW; Lee SG; Kim WK, Resorption of Autogenous Bone Graft in Cranioplasty: Resorption and Reintegration Failure. Korean J. Neurotrauma 2014, 10 (1), 10–14. [PubMed: 27169026]
3. (a) Aydin S; Kucukyuruk B; Abuzayed B; Aydin S; Sanus GZ, Cranioplasty: Review of materials and techniques. J. Neurosci. Rural Pract. 2011, 2 (2), 162–167; [PubMed: 21897681] (b) Aatman M. Shah; Henry Jung; Stephen Skirboll, Materials used in cranioplasty: a history and analysis. Neurosurg. Focus 2014, 36 (4), E19; [PubMed: 24684331] (c) Kneser U; Schaefer DJ; Polykandriotis E; Horch RE, Tissue engineering of bone: the reconstructive surgeon’s point of view. J. Cell. Mol. Med. 2006, 10 (1), 7–19. [PubMed: 16563218]
4. Shrivats AR; McDermott MC; Hollinger JO, Bone tissue engineering: state of the union. Drug Discov. Today 2014, 19 (6), 781–786. [PubMed: 24768619]

5. (a) Cao L; Cao B; Lu C; Wang G; Yu L; Ding J, An injectable hydrogel formed by in situ cross-linking of glycol chitosan and multi-benzaldehyde functionalized PEG analogues for cartilage tissue engineering. J. Mater. Chem. B 2015, 3 (7), 1268–1280;(b) Peter SJ; Kim P; Yasko AW; Yaszemski MJ; Mikos AG, Crosslinking characteristics of an injectable poly (propylene fumarate)/β-tricalcium phosphate paste and mechanical properties of the crosslinked composite for use as a biodegradable bone cement. J. Biomed. Mater. Res. A 1999, 44, 314–321;(c) Kim DY; Kwon DY; Kwon JS; Kim JH; Min BH; Kim MS, Stimuli-Responsive Injectable In situ-Forming Hydrogels for Regenerative Medicines. Polym. Rev. 2015, 55 (3), 407–452;(d) Prieto EM; Page JM; Harmata AJ; Guelcher SA, Injectable foams for regenerative medicine. WIREs Nanomed. Nanobiotechnol. 2014, 6 (2), 136–154;(e) Lee S-C; Wu C-T; Lee S-T; Chen P-J, Cranioplasty using polymethyl methacrylate prostheses. J. Clin. Neurosci. 2009, 16 (1), 56–63. [PubMed: 19046734]

6. Lendlein A; Behl M; Hiebl B; Wischke C, Shape-memory polymers as a technology platform for biomedical applications. Expert Rev. Med. Devices 2010, 7 (3), 357–379. [PubMed: 20420558]

7. (a) Behl M; Lendlein A, Shape-memory polymers. Mater. Today 2007, 10 (4), 20–28;(b) Wache H; Tartakowska D; Hentrich A; Wagner M, Development of a polymer stent with shape memory effect as a drug delivery system. J. Mater. Sci. Mater. Med. 2003, 14 (2), 109–112; [PubMed: 15348481] (c) Dailing EA; Nair DP; Setterberg WK; Kyburz KA; Yang C; D'Ovidio T; Anseth KS; Stansbury JW, Combined, Independent Small Molecule Release and Shape Memory via Nanogel-Coated Thiourethane Polymer Networks. Polym. Chem. 2016, 7 (4), 816–825. [PubMed: 27066114]

8. (a) Cui J; Kratz K; Heuchel M; Hiebl B; Lendlein A, Mechanically active scaffolds from radio-opaque shape-memory polymer-based composites. Polymer. Adv. Tech. 2011, 22 (1), 180–189;(b) Bao M; Lou X; Zhou Q; Dong W; Yuan H; Zhang Y, Electrospun biomimetic fibrous scaffold from shape memory polymer of PDLLA-co-TMC for bone tissue engineering. ACS Appl. Mater. Interfaces 2014, 6 (4), 2611–2621. [PubMed: 24476093]

9. (a) Zhang D; George OJ; Petersen KM; Jimenez-Vergara AC; Hahn MS; Grunlan MA, A bioactive "self-fitting" shape memory polymer scaffold with potential to treat cranio-maxillo facial bone defects. Acta Biomater. 2014, 10 (11), 4597–4605; [PubMed: 25063999] (b) Erndt-Marino JD; Munoz-Pinto DJ; Samavedi S; Jimenez-Vergara AC; Diaz-Rodriguez P; Woodard L; Zhang D; Grunlan MA; Hahn MS, Evaluation of the Osteoinductive Capacity of Polydopamine-Coated Poly (ε-caprolactone) Diacrylate Shape Memory Foams. ACS Biomater. Sci. Eng. 2015, 1 (12), 1220–1230.

10. (a) Wang S; Lu L; Gruetzmacher JA; Currier BL; Yaszemski MJ, Synthesis and characterizations of biodegradable and crosslinkable poly(ε-caprolactone fumarate), poly(ethylene glycol fumarate), and their amphiphilic copolymer. Biomaterials 2006, 27 (6), 832–841; [PubMed: 16102819] (b) Middleton JC; Tipton AJ, Synthetic biodegradable polymers as orthopedic devices. Biomaterials 2000, 21 (23), 2335–2346. [PubMed: 11055281]

11. Saini P; Arora M; Kumar MNVR, Poly(lactic acid) blends in biomedical applications. Adv. Drug Deliv. Rev. 2016, 107, 47–59. [PubMed: 27374458]

12. (a) Nampoothiri KM; Nair NR; John RP, An overview of the recent developments in polylactide (PLA) research. Bioresour. Technol. 2010, 101 (22), 8493–8501; [PubMed: 20630747] (b) Garlotta D, A literature review of poly (lactic acid). J. Polym. Environ. 2001, 9 (2), 63–84.

13. Lebourg M; Antón JS; Ribelles JLG, Porous membranes of PLLA–PCL blend for tissue engineering applications. Eur. Polym. J. 2008, 44 (7), 2207–2218.

14. (a) Sadiasa A; Nguyen TH; Lee B-T, In vitro and in vivo evaluation of porous PCL-PLLA 3D polymer scaffolds fabricated via salt leaching method for bone tissue engineering applications. J. Biomater. Sci. Polym. Ed. 2014, 25 (2), 150–167; [PubMed: 24138179] (b) Guarino V; Causa F; Taddei P; di Foggia M; Ciapetti G; Martini D; Fagnano C; Baldini N; Ambrosio L, Polylactic acid fibre-reinforced polycaprolactone scaffolds for bone tissue engineering. Biomaterials 2008, 29 (27), 3662–3670; [PubMed: 18547638] (c) Todo M; Park J-E; Kuraoka H; Kim J-W; Taki K; Ohshima M, Compressive deformation behavior of porous PLLA/PCL polymer blend. J. Mater. Sci. 2009, 44 (15), 4191–4194;(d) Gaona LA; Gómez Ribelles JL; Perilla JE; Lebourg M, Hydrolytic degradation of PLLA/PCL microporous membranes prepared by freeze extraction. Polym. Degrad. Stab. 2012, 97 (9), 1621–1632;(e) Liao G; Jiang S; Xu X; Ke Y, Electrospun aligned PLLA/PCL/HA composite fibrous membranes and their in vitro degradation behaviors. Mater. Lett. 2012, 82, 159–162;(f) Torabinejad B; Mohammadi-Rovshandeh J; Davachi SM; Zamanian A, Synthesis and characterization of nanocomposite scaffolds based on triblock

copolymer of l-lactide, ε-caprolactone and nano-hydroxyapatite for bone tissue engineering. Mater. Sci. Eng. C 2014, 42, 199–210.

15. (a) Weng W; Song S; Cao L; Chen X; Cai Y; Li H; Zhou Q; Zhang J; Su J, A comparative study of bioartificial bone tissue poly-l-lactic acid/polycaprolactone and PLLA scaffolds applied in bone regeneration. J. Nanomater. 2014, 2014, 236;(b) Holmbom J; Södergård A; Ekholm E; Märtson M; Kuusilehto A; Saukko P; Penttinen R, Long-term evaluation of porous poly(ϵ-caprolactone-co-L-lactide) as a bone-filling material. J. Biomed. Mater. Res. A 2005, 75A (2), 308–315.
16. (a) Passos MF; Fernández-Gutiérrez M; Vázquez-Lasa B; Román JS; Filho RM, PHEMA-PLLA semi-interpenetrating polymer networks: A study of their swelling kinetics, mechanical properties and cellular behavior. Eur. Polym. J. 2016, 85, 150–163;(b) Mandal B; Ray SK; Bhattacharyya R, Synthesis of full and semi Interpenetrating hydrogel from polyvinyl alcohol and poly (acrylic acid-co-hydroxyethylmethacrylate) copolymer: Study of swelling behavior, network parameters, and dye uptake properties. J. Appl. Polym. Sci. 2012, 124 (3), 2250–2268;(c) Lumelsky Y; Zoldan J; Levenberg S; Silverstein MS, Porous Polycaprolactone−Polystyrene Semi-interpenetrating Polymer Networks Synthesized within High Internal Phase Emulsions. Macromolecules 2008, 41 (4), 1469–1474.
17. Frisch KC; Klempner D; Frisch HL, Recent advances in interpenetrating polymer networks. Polym. Eng. Sci. 1982, 22 (17), 1143–1152.
18. Shibita A; Takase H; Shibata M, Semi-interpenetrating polymer networks composed of poly(l-lactide) and diisocyanate-bridged 4-arm star-shaped ε-caprolactone oligomers. Polymer 2014, 55 (21), 5407–5416.
19. Woodard LN; Page VM; Kmetz KT; Grunlan MA, PCL–PLLA Semi-IPN Shape Memory Polymers (SMPs): Degradation and Mechanical Properties. Macromol. Rapid Commun. 2016, 37 (23), 1972–1977. [PubMed: 27774684]
20. Nail L; Zhang D; Reinhard J; Grunlan M, Fabrication of a Bioactive, PCL-based" Self-fitting" Shape Memory Polymer Scaffold. J. Vis. Exp.: JoVE 2014, (105).
21. Pitt CG; Chasalow F; Hibionada Y; Klimas D; Schindler A, Aliphatic polyesters. I. The degradation of poly (ϵ-caprolactone) in vivo. J. Appl. Polym. Sci. 1981, 26 (11), 3779–3787.
22. Siparsky GL; Voorhees KJ; Dorgan JR; Schilling K, Water transport in polylactic acid (PLA), PLA/ polycaprolactone copolymers, and PLA/polyethylene glycol blends. J. Environ. Polym. Degr. 1997, 5 (3), 125–136.
23. (a) Hearon K; Singhal P; Horn J; Small W; Olsovsky C; Maitland KC; Wilson TS; Maitland DJ, Porous Shape-Memory Polymers. Polym. Rev. 2013, 53 (1), 41–75;(b) Ashby MF; Medalist RFM, The mechanical properties of cellular solids. Metall. Trans. A 1983, 14 (9), 1755–1769.
24. Wang S; Kempen DHR; de Ruiter GCW; Cai L; Spinner RJ; Windebank AJ; Yaszemski MJ; Lu L, Molecularly Engineered Biodegradable Polymer Networks with a Wide Range of Stiffness for Bone and Peripheral Nerve Regeneration. Adv. Funct. Mater. 2015, 25 (18), 2715–2724.
25. Zhang D; Petersen KM; Grunlan MA, Inorganic–organic shape memory polymer (SMP) foams with highly tunable properties. ACS Appl. Mater. Interfaces 2012, 5 (1), 186–191. [PubMed: 23227875]
26. Tobushi H; Hara H; Yamada E; Hayashi S, Thermomechanical properties in a thin film of shape memory polymer of polyurethane series. Smart Mater. Struct. 1996, 5 (4), 483.
27. (a) Tsuji H; Ikada Y, Blends of aliphatic polyesters. II. Hydrolysis of solution-cast blends from poly (L-lactide) and poly (E-caprolactone) in phosphate-buffered solution. J. Appl. Polym. Sci. 1998, 67 (3), 405–415;(b) Qian H; Bei J; Wang S, Synthesis, characterization and degradation of ABA block copolymer of l-lactide and ε-caprolactone. Polym. Degrad. Stab. 2000, 68 (3), 423–429.
28. (a) Tsuji H; Ikada Y, Properties and morphology of poly(L-lactide). II. Hydrolysis in alkaline solution. J. Polym. Sci., Part A: Polym. Chem. 1998, 36 (1), 59–66;(b) von Burkersroda F; Schedl L; Göpferich A, Why degradable polymers undergo surface erosion or bulk erosion. Biomaterials 2002, 23 (21), 4221–4231. [PubMed: 12194525]
29. Htay AS; Teoh SH; Hutmacher DW, Development of perforated microthin poly(ε-caprolactone) films as matrices for membrane tissue engineering. J. Biomater. Sci. Polym. Ed. 2004, 15 (5), 683–700. [PubMed: 15264668]

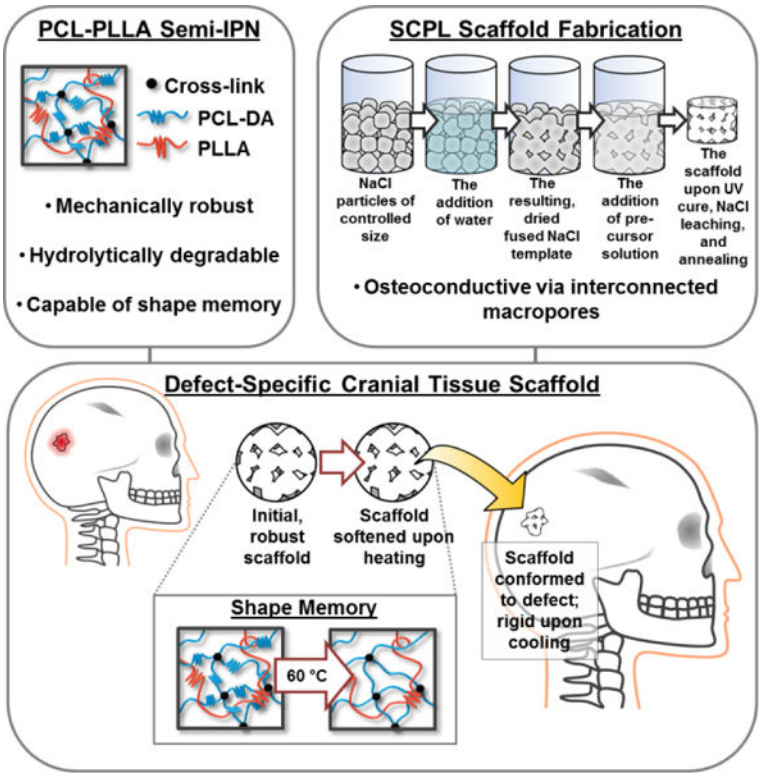

Figure 1.

Summary of the porous PCL-PLLA semi-IPN scaffold design. The unique PCL-PLLA semi-IPN structure and the fabrication-induced macropores contribute to a cranial tissue scaffold with enabling material properties that's capable of achieving defect-specific geometries.

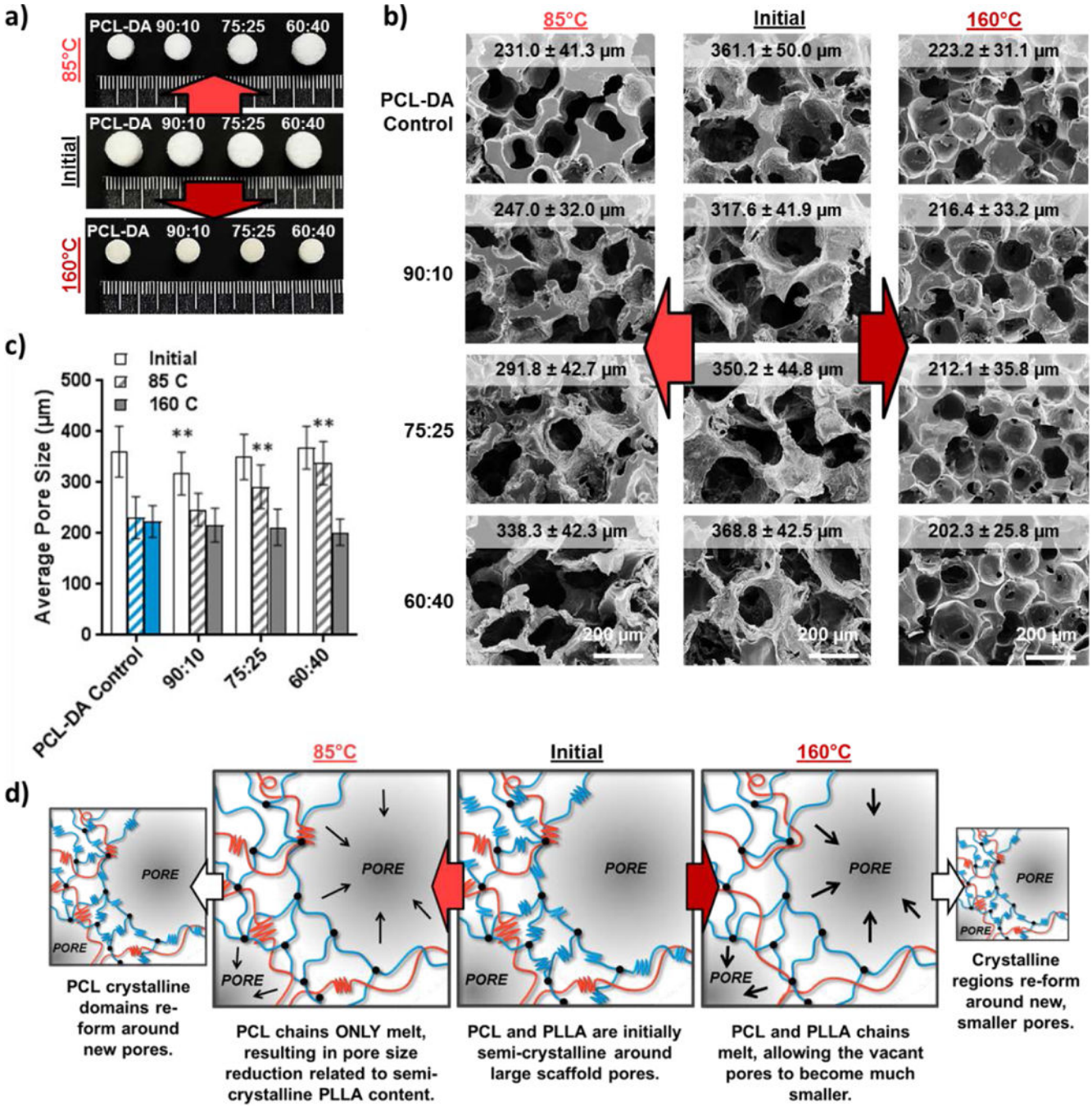

Figure 2.

Effect of annealing/annealing temperature (85 and 160 °C) on PCL-PLLA semi-IPN and PCL-DA control scaffolds (PCL-DA; n = 25). a) Scaffold diameter before and after annealing. b) SEM images of scaffold cross-sections before and after annealing. c) Average pore size before and after annealing (**p < 0.01 vs corresponding PCL-DA control). d) Schematic representation of the morphological response to annealing temperature.

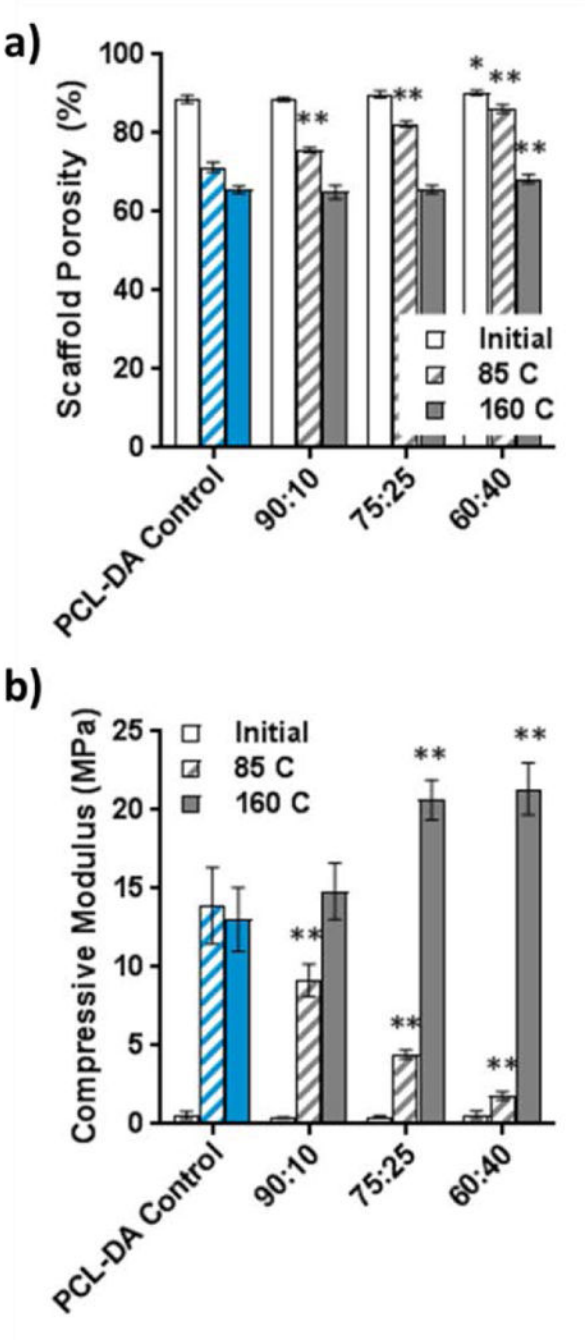

Figure 3.

For scaffolds based on PCL-DA (n = 25): a) Porosity before and after annealing by temperature (*p < 0.05, **p < 0.01 vs corresponding PCL-DA control). b) Compressive modulus before and after annealing by temperature (**p < 0.01 vs corresponding PCL-DA control).

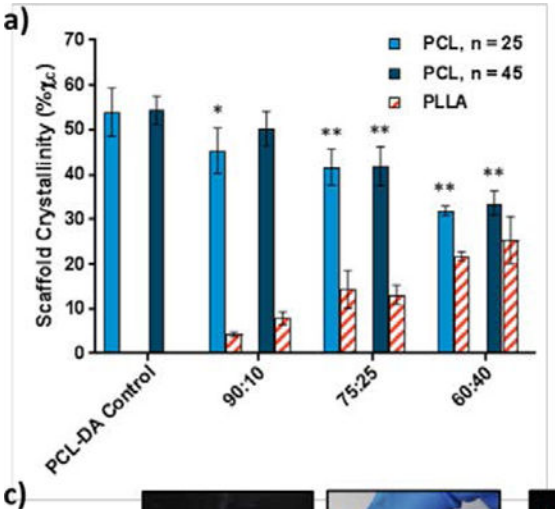

b)

		1st Cycle		2nd Cycle	
		R_f	R_r	R_f	R_r
n = 25	PCL-DA	101.9 ± 0.1	89.6 ± 2.6	101.8 ± 0.1	99.8 ± 0.3
	90:10	101.8 ± 0.0	58.1 ± 2.4**	101.8 ± 0.1	103.1 ± 2.1**
	75:25	101.8 ± 0.1	81.9 ± 7.1*	101.6 ± 0.1*	99.7 ± 0.5
	60:40	101.1 ± 0.0**	33.0 ± 2.7**	101.1 ± 0.1**	92.4 ± 0.8**
n = 45	PCL-DA	101.2 ± 0.6++	55.2 ± 8.8++	101.1 ± 0.3++	95.3 ± 1.9++
	90:10	100.6 ± 0.3**++	35.3 ± 5.6**++	100.7 ± 0.3**++	95.2 ± 0.7++
	75:25	101.2 ± 0.2++	30.0 ± 1.1**++	101.3 ± 0.1+	94.2 ± 1.2++
	60:40	101.2 ± 0.1	30.3 ± 2.4**	101.3 ± 0.0	88.4 ± 1.1**++

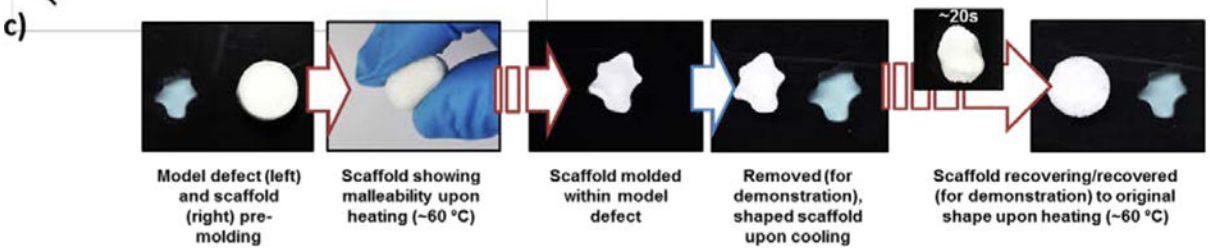

Figure 4.

a) PCL and PLLA % crystallinity values for PCL-PLLA semi-IPN and PCL-DA control scaffolds (*p < 0.05, **p < 0.01 vs corresponding PCL-DA control). b) Shape fixity (R_f) and shape recovery (R_r) values of scaffolds over two cycles (*p < 0.05, **p < 0.01 vs corresponding PCL-DA control; +p < 0.05, ++p < 0.01 vs corresponding PCL-DA (n = 25) scaffold). c) Simulation of the defect-specific implantation of a SMP scaffold within a model defect.

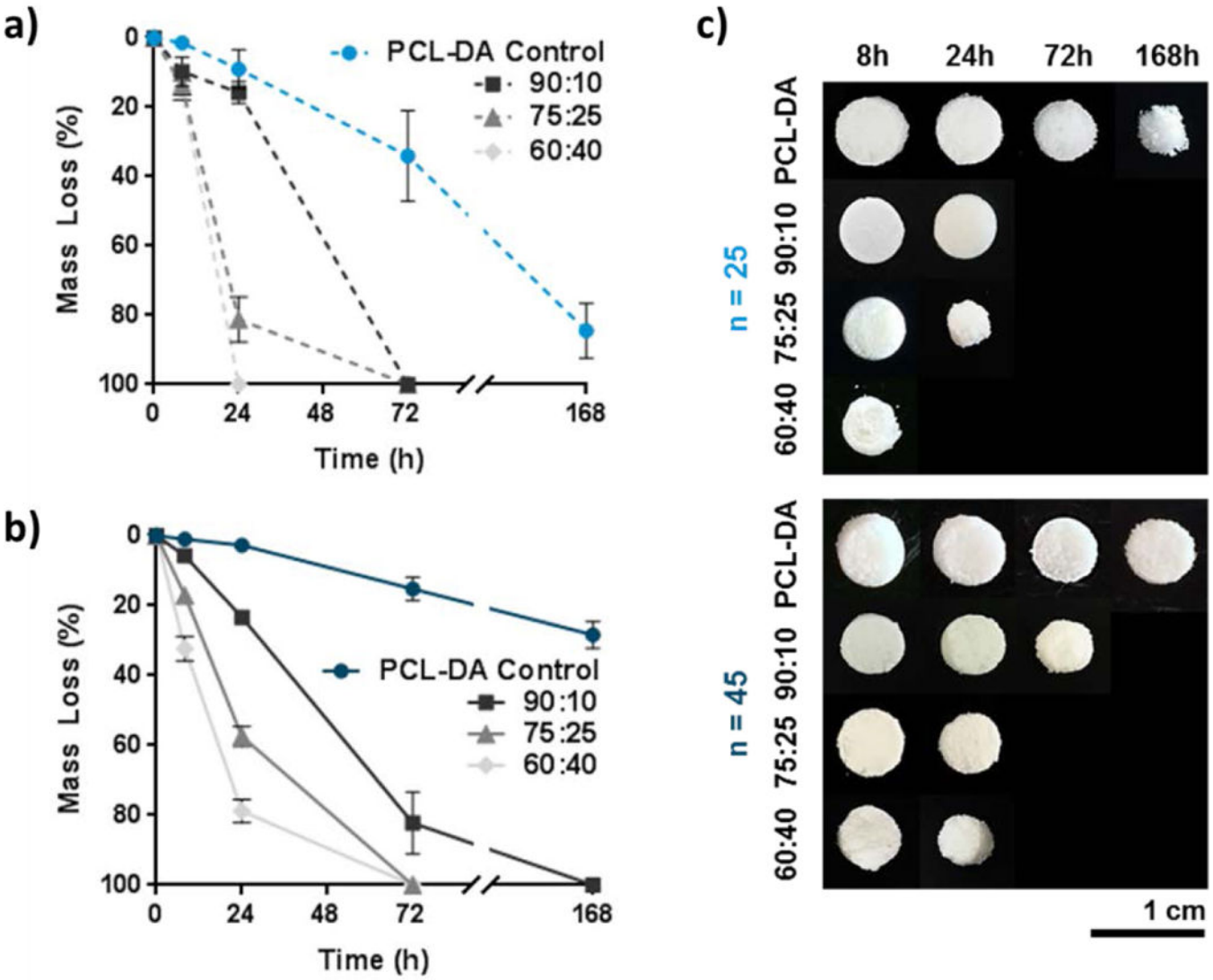

Figure 5.

Mass loss under accelerated conditions (1 M NaOH, 37 °C) for PCL-PLLA semi-IPN and PCL-DA control scaffolds based on a) PCL-DA (n = 25) and b) PCL-DA (n = 45). c) Images of scaffolds during degradation.

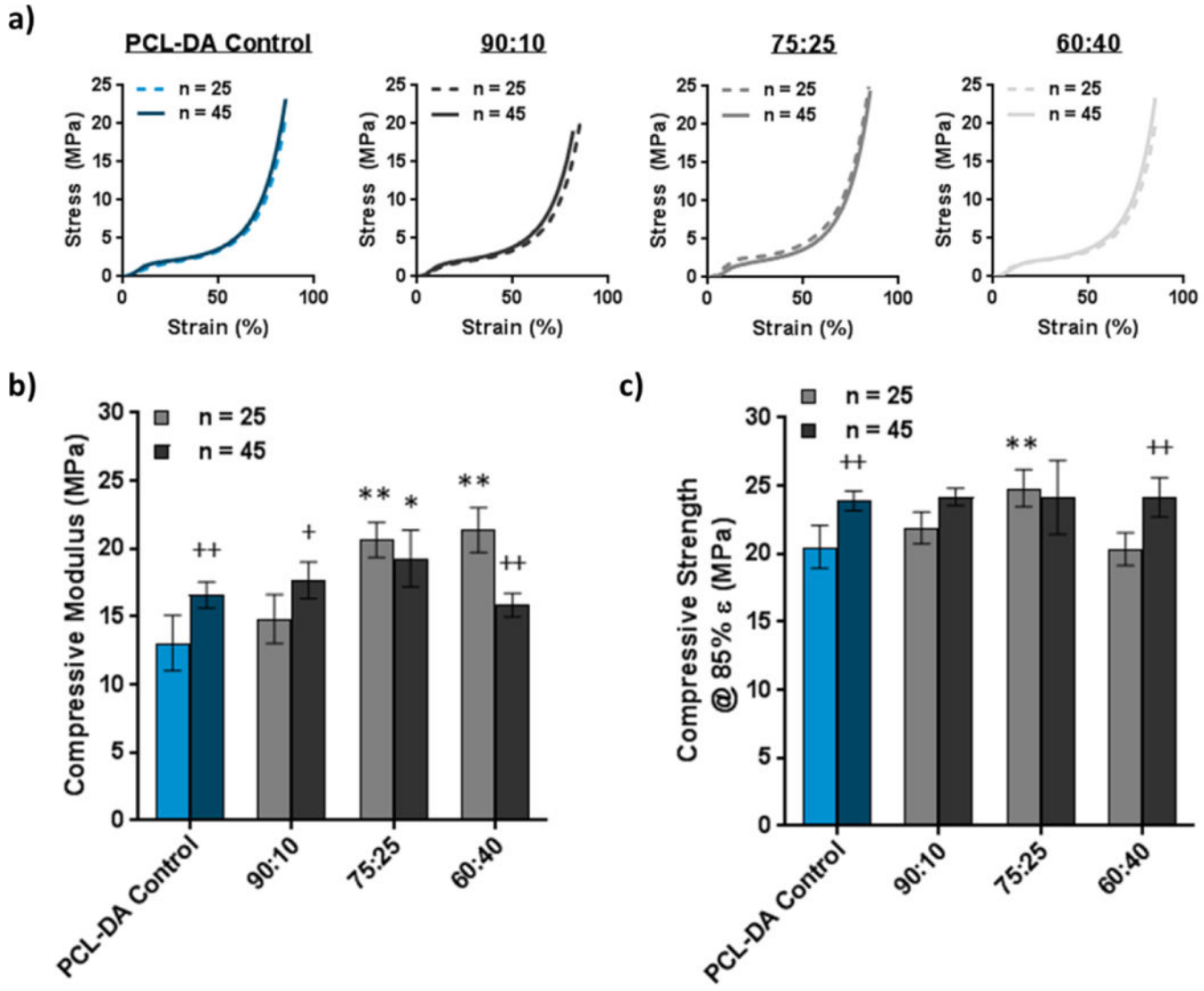

Figure 6.

a) Stress-strain curves for PCL-PLLA semi-IPN and PCL-DA control scaffolds. b) Compressive modulus (E) values of SMP scaffolds (*$p < 0.05$, **$p < 0.01$ vs corresponding PCL-DA control; +$p < 0.05$, ++$p < 0.01$ vs corresponding PCL-DA (n = 25) scaffold). c) Compressive strength (CS) values at 85% stain of SMP scaffolds (**$p < 0.01$ vs corresponding PCL-DA control; ++$p < 0.01$ vs corresponding PCL-DA (n = 25) scaffold).